

TRANSFERRED SUBSTRATE HETEROJUNCTION BIPOLAR TRANSISTORS FOR SUBMILLIMETER WAVE APPLICATIONS

Andy Fung, Lorene Samoska, Peter Siegel
California Institute of Technology Jet Propulsion Laboratory, Pasadena, CA 91109, USA

Mark Rodwell, Miguel Urteaga, Vamsi Paidi
Department of Electrical and Computer Engineering, University of California, Santa
Barbara, CA 93106, USA

Roger Malik
RJM Semiconductor, Berkeley Heights, NJ 07922, USA

ABSTRACT

We present ongoing work towards the development of submillimeter wave transistors with goals of realizing advanced high frequency amplifiers, voltage controlled oscillators, active multipliers, and traditional high-speed digital circuits. The approach involves fabrication of indium phosphide heterojunction bipolar transistors in a low parasitic transferred-substrate process, with the necessary requirements in uniformity and reliability for eventual space-borne applications. Transferred Substrate Heterojunction Bipolar Transistors (TSHBTs) have previously demonstrated record >20 dB measured unilateral power gain at 100 GHz, and high power gains in the 140-220 GHz band [1]. Single-transistor amplifiers have shown 6.3 dB gain at 174 GHz [2]. Thus far we have completed a first generation of TSHBTs with large emitter stripes of $0.8 \times 6 \mu\text{m}^2$. S-parameter measurements resulted in an extrapolated power gain cutoff frequency (F_{max}) of 150 GHz and current gain cutoff frequency (F_c) of 110 GHz, at an emitter current density of 94 kA/cm^2 and collector-emitter bias voltage of 1.25V. Future generations of TSHBTs will target improvements in speed, uniformity and reliability, through better semiconductor layer structure design and epitaxial material quality, reduction in transistor geometry size, and refinements in fabrication procedures.

Introduction and Background

Indium phosphide (InP) heterojunction bipolar transistors (HBTs) are one of the most prevalent high performance transistor technologies available. Advantages of this technology arise from the precise control of the semiconductor epitaxial structure that electrons traverse through and the material properties of the epitaxy. In HBTs, electrons move in the direction of epitaxial growth, as a result, the environment of the electrons at each region of the transistor can be more easily and accurately controlled for optimal performance within the narrowest spatial dimensions. Some advantages resulting from this are that the epitaxial material for InP HBTs can be grown with a large bandgap emitter region to reduce injection of holes from the base into the emitter that decreases gain, an alloy or doping graded base region can be grown in the epitaxy to produce a built in electric field to increase electron transport speed. Also through epitaxial growth a high voltage breakdown material such as InP can be produced for the collector region so that the transistor may operate at higher voltages (see Figure 1). In contrast, in other high speed transistor technologies, such as high electron mobility transistors (HEMTs), the electrons travel perpendicular to the direction of epitaxial growth, confined to particular material layers of fixed properties. Modifications for material properties in the direction of electron transport for improving performance can only be done via processes after epitaxial growth, generally with less precision and more complications. Silicon Germanium HBTs, another high speed technology, consists of semiconductor materials with lower breakdown voltages and are less suitable for power applications. InP HBTs are well suited for both high speed and high output power operation, which is desired for our applications.

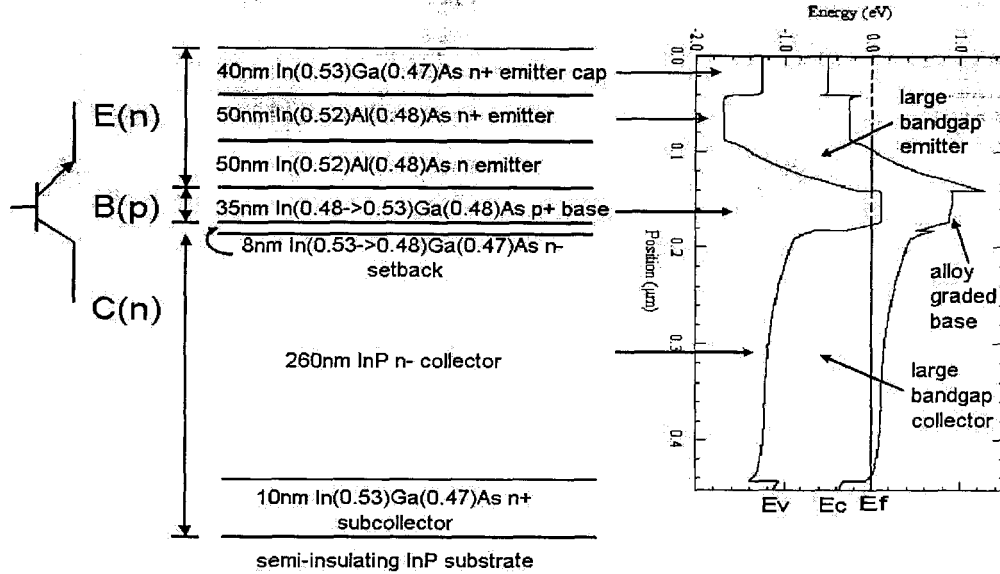


Figure 1: Schematic representations of an indium aluminum arsenide (InAlAs) emitter, indium gallium arsenide (InGaAs) base, InP collector, double heterojunction bipolar transistor (DHBT). The large bandgap emitter provides a larger energy barrier for holes from injecting from the base into the emitter in forward active operation that would decrease gain. The base is alloy graded to provide a built-in electric field to speed electrons through the base into the collector. The collector is made of a large bandgap material to withstand larger voltages before breakdown. The energy (eV) versus position (μm) diagram is simulated using Bandprofiler developed by W.Frensley UTDallas.

Motivation

The goal of this effort is to develop the fastest reliable transistor process beyond what is available from industry and have the capability to easily add features for performance not typically allowed in foundry services that are fixed. We are pursuing HBTs as they have shown thus far to have the highest power gain, >20 dB at 100 GHz [1] and higher power handling capability due to epitaxial engineering of the collector region of the transistor, in contrast to HEMTs. We expect that HBTs will provide more power per area at higher frequencies than HEMTs, and will yield higher transistor count ICs due to its particular fabrication procedures. To date InP HBTs have demonstrated ICs with transistor counts approaching five thousand [3]. With the successful implementation of an ultra-high-speed and high-power HBT we plan to fabricate power amplifiers where they may be integrated into local oscillator chains for space heterodyne systems [4]. Additionally, voltage controlled oscillators can be fabricated to simplify local oscillator chains by reducing component count and size (see Figure 2). Ultimately we would like to have a high yield process so that we can develop ultra-high speed mixed-signal ICs. Systems that we would like to utilize this technology in are for THz imaging systems, which are in development at JPL (see Figure 3) [5], and also future space hardware such as advanced autocorrelators for high-resolution remote sensing spectral analysis.

Transferred Substrate for Improving InP HBT Performance

The high frequency figures of merit of HBTs are the current gain cutoff frequency (F_t) and maximum frequency of oscillation (power gain cutoff frequency) (F_{max}). Physically, F_t can be expressed as,

$$F_t = 1/(2 \cdot \pi \cdot \tau_{\text{ec}}) \approx 1/(2 \cdot \pi \cdot (\tau_{\text{e}} + \tau_{\text{b}} + \tau_{\text{bc}} + \tau_{\text{c}})) \quad (1)$$

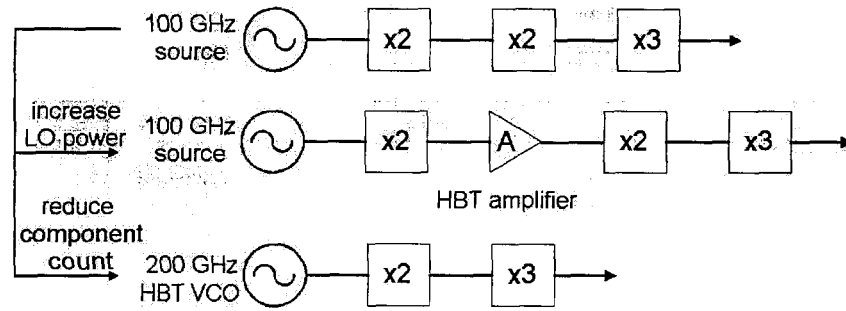


Figure 2: Block diagram of implementations of an 1.2 THz local oscillator (LO) chain. A baseline version is shown at the top. HBTs can be inserted along the chain to increase power. HBTs can also be used to produce high frequency voltage controlled oscillators to simplify LOs by reducing component counts.

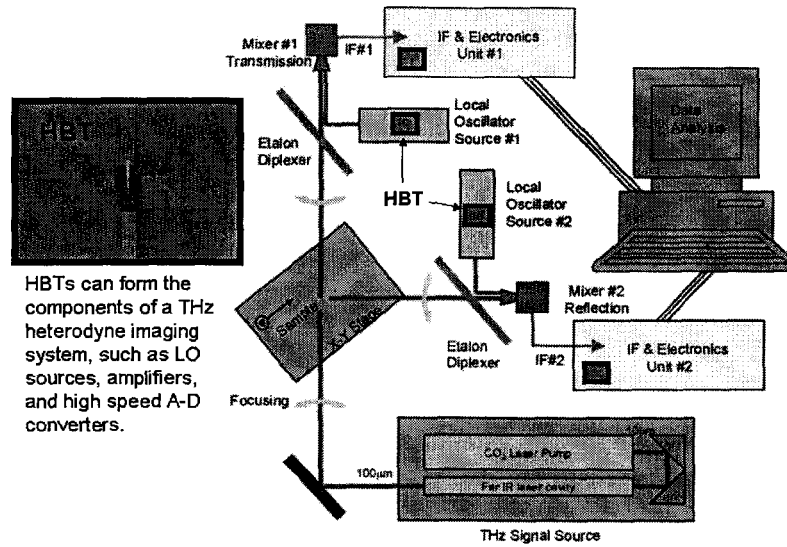


Figure 3: Schematic of a scanned pixel terahertz imager system under development at JPL. HBTs are displayed in components where they can improve system performance.

where, τ_{ec} is the total emitter to collector delay time, τ_e is the emitter charging time, τ_b is the base transit time, τ_{bc} is the base-collector junction transit time, and τ_c is the collector charging time [6]. The power gain cutoff frequency can be approximated by,

$$F_{max} \geq (F_t / (8 \cdot \pi \cdot R_b \cdot C_{cb}))^{1/2} \quad (2)$$

Where R_b is the complete base resistance from base contact to the base layer under the emitter, and C_{cb} is the full base to collector capacitance. F_{max} can be more accurately calculated with $R_b \cdot C_{cb}$ modeled by an effective time constant of a distributed network of the base-collector region [1]. Comparing the typical mesa HBT (Figure 4 (a)) and the Transferred Substrate HBT (TSHBT) (Figure 4 (b)), the TSHBT method overcomes the limitation of the base-collector overlap inherent to the mesa HBT since the collector contact is independently defined from the backside of the wafer. By minimizing C_{cb} , F_{max} is improved. To increase both F_t and F_{max} simultaneously, scaling in the vertical direction minimizes transit times in F_t , however this increases intrinsic and parasitic resistances and capacitances. To reduce these resistances and capacitances to increase both F_t and F_{max} the transistor must also be scaled in the horizontal direction and doped higher. Each of these fabrication degrees of freedom self limit each other to the point that they are allowed by material and equipment capabilities.

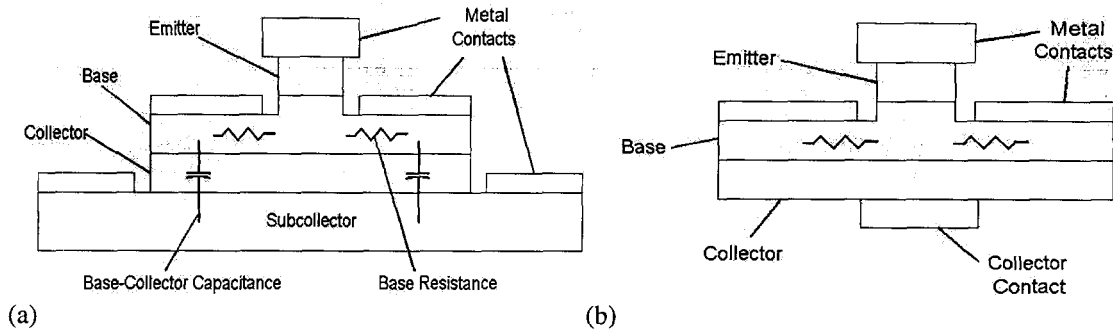


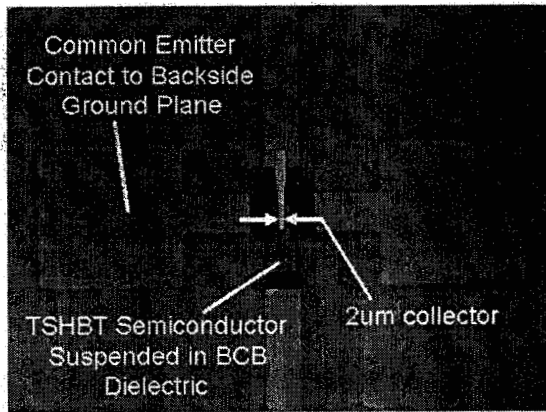
Figure 4: (a) Schematic cross section of a typical mesa HBT. (b) Schematic cross section of a TSHBT.

Experimentally, F_t and F_{max} are typically extrapolated from lower frequency measurements to the higher cutoff frequency values, due to the limited bandwidth of characterization setups. F_t is determined from the current gain H_{21} and F_{max} from Mason's unilateral power gain (U), both cutoff frequencies are determined from the frequency value where the gain curves reach 0 dB. H_{21} and U, as a function of frequency, are mathematically derived from S-parameter measurements over frequency. Cutoff frequencies are typically extrapolated from lower frequencies with a -20db/decade gain behavior based on the single pole frequency response of the hybrid- π circuit model [7]. Recently, studies have indicated that the simple hybrid- π model may not properly fit certain HBTs operated in particular regimes [8-11]. Physical phenomena such as electron velocity modulation in the base-collector depletion region resulting in a reduction of the base-collector capacitance [10], and hole transport response in the collector region under base pushout [11] have been attributed to the deviation from the simple hybrid- π model. In this report the measured data appears to fit the simple hybrid- π model, so for the purpose of comparisons, F_t and F_{max} are determined based on the standard extrapolation with a -20 db/decade trend.

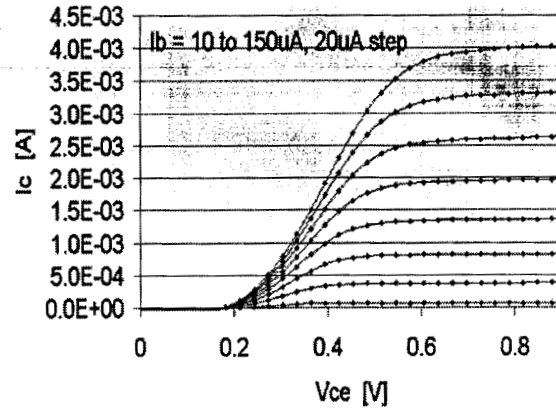
Development of Transferred Substrate InP HBTS at JPL

At JPL we are in collaboration with UCSB and RJM Semiconductor in an effort to develop advanced high speed and high reliability HBT processes for implementing advanced amplifiers, VCOs and traditional digital circuits for THz imagers and spectrometers. In the Microdevices Laboratory we recently fabricated the first wafer run of TSHBTs at JPL (Figure 5 (a)). The epitaxial material used for the TSHBTs is of a single heterojunction InAlAs emitter, and InGaAs base and collector design. The base is 400 \AA thick carbon doped $5 \times 10^{19}\text{ cm}^{-3}$. Dc measurements of the collector current versus collector-emitter voltage for different base current shows maximum small signal current gain β of 36 (Figure 5 (b)). From S-parameter measurements we deduce maximum F_t and F_{max} of 110 and 150 GHz, respectively, at an emitter current density of 94 kA/cm^2 (Figure 5 (c)). Through improvements in epitaxial designs, epitaxial material quality, and improvements in microfabrication, we expect to incrementally improve TSHBT performance. Future transistors will utilize DHBT epitaxy for higher power handling capability.

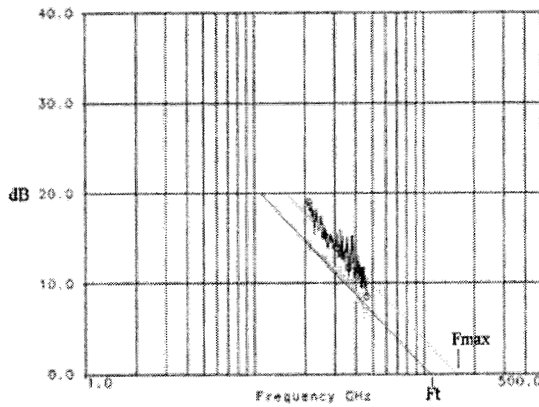
The present TSHBT process includes 9 stepper lithography mask steps and two electron-beam lithography direct writes for the emitter and collector contacts. Important in the process is the deposition of a 5 \mu m thick low dielectric Benzocyclobutene (BCB) resin that serves as an intermediate substrate supporting the HBTs and passive components, from the ground plane. The integrated passive nickel-chrome resistors and metal-insulator-metal capacitors provide for a MMIC process (Figure 6). In developing the TSHBT process at JPL, a large-feature-size reduced-process-step HBT process for evaluating dc epitaxial material quality, and a rf mesa HBT process for developing all necessary top-side wafer processes for TSHBTs have also been implemented [12]. Table 1 summarizes rf data we have measured thus far from both rf mesa and TSHBT processes. In the table the samples that are used have nominally the same epitaxial design. Wafer 1, 2 and 3 used in the mesa process differ in that wafers 1 and 2 have nominal base doping of $4 \times 10^{19}\text{ cm}^{-3}$ and wafer 3 has base doping of $5 \times 10^{19}\text{ cm}^{-3}$. Wafer 4, used in the TSHBT process is identical to wafer 3, except that there is no subcollector layer. Comparing the cutoff frequency values for wafers 3 and 4, F_{max} has improved in the TSHBT sample as theory would suggests.



(a)

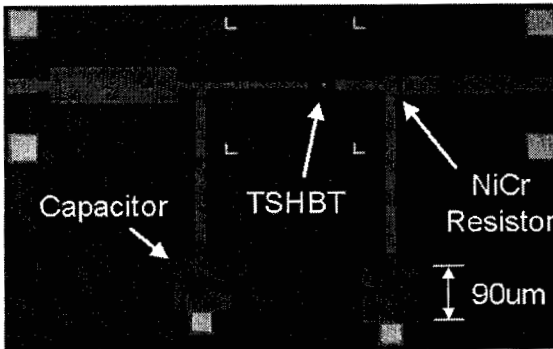


(b)

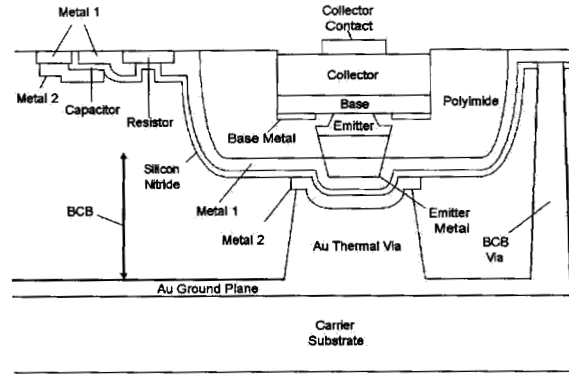


(c)

Figure 5: (a) Optical photo of an InP TSHBT. The emitter stripe is $0.8 \times 6 \mu\text{m}^2$ and collector stripe is $2 \times 8 \mu\text{m}^2$ (b) Dc I_c versus V_{ce} for different I_b of InP TSHBT. Maximum small signal β is 36. (c) Gain plots of an InP TSHBT deduced from S-parameter measurements. F_t and F_{max} are 110 and 150 GHz, respectively at an emitter current density J_e of 94 kA/cm^2 and V_{ce} 1.25V.



(a)



(b)

Figure 6: (a) Optical photo of a 200 GHz TSHBT amplifier during fabrication showing integrated TSHBT, resistors and capacitors. (b) Cross section (not drawn to scale) of transferred substrate MMIC process.

	Wafer 1, beryllium base, mesa HBT	Wafer 2, carbon base, mesa HBT	Wafer 3, carbon base, mesa HBT	Wafer 4, carbon base, TSHBT
F_t [GHz]	126	122	108	110
F_{max} [GHz]	120	100	115	150

Table 1: Summary of measured rf mesa HBTs and TSHBTs fabricated at JPL. F_t and F_{max} for each wafer sample is measured simultaneously under the same bias conditions.

Acknowledgments

The research and development presented in this paper was carried out at the California Institute of Technology Jet Propulsion Laboratory, a federally funded research and development center under a contract with the National Aeronautics and Space Administration, and by MDA under contract DTRA01-01-0222, managed by DTRA. The authors thank Richard Muller, Paul Maker and Pierre Echternach, at JPL for providing electron beam lithography.

References

- [1] M. Rodwell, et al., *IEEE Trans. Electron Devices*, vol. 48, Nov. 2001.
- [2] M. Urteaga, et al., *Proc. IEEE GaAs IC Symp.*, Oct. 2001.
- [3] <http://www.vitesse.com/news/20030113.shtml>, Jan. 2003.
- [4] J. Ward, et al., *Proceedings 14th Inter. Symp. on Space Terahertz Tech.*, 2003 (to be published).
- [5] P.H. Siegel, "Submillimeter-Wave Camera," *JPL New Technology Report NPO20718*, June 1, 1999.
- [6] B. Jalali and S. Pearton, *InP HBTs Growth, Processing, and Applications*, Artech House Inc., 1995.
- [7] S. Sze (ed.), *Modern Semiconductor Device Physics*, John Wiley & Sons Inc., 1998.
- [8] M. Urteaga, et al., (to be published).
- [9] B. Willen, et al., *IEEE Electron Device Lett.*, vol. 23, Oct. 2002.
- [10] Y. Betser, et al., *IEEE Trans. Electron Devices*, vol. 46, Apr. 1999.
- [11] M. Rohner, et al., *IEEE Trans. Electron Devices*, vol. 49, Feb. 2002.
- [12] A. Fung, et al., *Proceedings FAR-IR, SUB-MM & MM DETECTOR TECHNOLOGY WORKSHOP*, Wolf J., Farhoomand J. and McCreight C.R. (eds.), NASA/CP-211408, 2002 (in press).